JMEPEG (2008) 17:580–585
DOI: 10.1007/s11665-007-9141-0

©ASM International
1059-9495/$19.00

Relationship Between Crystalline Structure and Hardness of Ti-Si-N-O Coatings Fabricated by dc Sputtering

Leandro García-González, Julián Hernández-Torres, Claudia Mendoza-Barrera, Miguel Meléndez-Lira, Pedro J. García-Ramírez, Jaime Martínez-Castillo, Ángel Sauceda, Agustin L. Herrera-May, Juan Muñoz Saldaña, and Francisco J. Espinoza-Beltrán

(Submitted November 15, 2006; in revised form May 29, 2007)

Ti-Si-N-O coatings were deposited on AISI D2 tool steel and silicon substrates by dc reactive magnetron co-sputtering using a target of Ti-Si with a constant area ratio of 0.2. The substrate temperature was 400 °C and reactive atmosphere of nitrogen and argon. For all samples, argon flow was maintained constant at 25 sccm, while the flow of the nitrogen was varied to analyze the structural changes related to chemical composition and resistivity. According to results obtained by x-ray diffraction and stoichiometry calculations by x-ray energy dispersive spectroscopy the Ti-Si-N-O coatings contain two solid solutions. The higher crystalline part corresponds to titanium oxynitrure. Hardness tests on the coatings were carried out using the indentation work model and the hardness value was determined. Finally, the values of hardness were corroborated by nanoindentation test, and values of Young's modulus and elastic recovery were discussed. We concluded that F2TSN sample (F_{Ar} = 25 sccm, F_N = 5 sccm, P = 200 W, and $P_W = 8.9 \times 10^{-3}$ mbar) presented the greatest hardness and the lowest resistivity values, due to its preferential crystalline orientation.

Keywords crystalline, hardness, TiSiNO, XRD

1. Introduction

Research and technological developments are fundamental to satisfying the society's demands for new and high-quality technological products. To effectively prevent the diffusion of the copper into dielectric material and silicon substrate, in integrated circuits, it is necessary to develop materials with high hardness and low resistivity. In this way, intrinsical, thermal, and electrical stresses due to copper can be avoided. It has been reported that ternary systems as TiSiN (Ref 1, 2), WSiN (Ref 3, 4), and TaSiN (Ref 5, 6) are able to substitute the TiN (Ref 7, 8) as diffusion barrier in dielectric device fabrication due to their improving properties. MeSiN (Me: transition metal) materials usually present mixed microstructure formed by a nanocrystalline phase embedded in amorphous matrix, generally of silicon nitride (Ref 9, 10).

Also, Ti-Si-N-O coatings have been fabricated to act as a diffusion barrier (Ref 11, 12) due to their promising properties, which make them strong candidates for the next generation of diffusion barriers in CMOS technology. Smith and Custer (Ref 13), found that resistivity varies from 400 μΩ cm for TiN to 1×10^6 μΩ cm for Ti-Si-N. Ee et al. (Ref 14) obtained resistivity values from 3.63×10^3 μΩ cm to up to 6.45×10^6 μΩ cm for the system Ti-Si-N-O fabricated by rf reactive magnetron sputtering. Studies carried out on this quaternary system reveal that these coatings consist of nanocrystals generally absorbed in amorphous phases of Ti-O, Si-O, Si-N, and Si-N-O (Ref 12). Shalaeva accomplished a complete study related to the composition of phases of Ti-Si-N-O coatings (Ref 12). A metastable phase diagram was established comparing the ternary equilibrium diagrams of Ti-Si-N and Ti-Si-O. Other authors have focused their study on the resistivity of this quaternary system and its dependence on growing parameters. In addition, the microstructure, superficial morphology, roughness, and chemical bonding types of this quaternary system have been studied. However, a study on the hardness of these coatings due to a controlled variation of the nitrogen flow has not yet been reported. In this paper, we report the development and analysis of Ti-Si-N-O coatings through the use of dc reactive magnetron sputtering. The structural and morphological characterization and composition were carried out using x-ray diffraction (XRD), x-ray energy dispersive spectroscopy (EDS), atomic force microscopy (AFM), scanning electron microscopy (SEM), and Raman spectroscopy while the hardness was studied via indentations work model.

Leandro García-González, Claudia Mendoza-Barrera, Pedro J. García-Ramírez, Jaime Martínez-Castillo, Ángel Sauceda, and **Agustin L. Herrera-May,** Centro de Investigación en Micro y Nanotecnología, Universidad Veracruzana, Boca del Rio, Veracruz, Mexico; **Julián Hernández-Torres,** Universidad del Papaloapan, Campus Loma Bonita, Loma Bonita, Oaxaca, Mexico; **Miguel Meléndez-Lira,** Departamento de Física, Centro de Investigación y de Estudios Avanzados del IPN, Mexico DF, Mexico; **Juan Muñoz Saldaña** and **Francisco J. Espinoza-Beltrán,** Centro de Investigación y de Estudios Avanzados del IPN, Unidad Querétaro, Queretaro, Mexico. Contact e-mail: leagarcia@uv.mx.

2. Experimental

Ti-Si-N-O coatings were fabricated using a dc magnetron reactive sputtering system (model Intercovamex-sputtering V3), with a target of Ti (purity of 99.99%) and a small area of c-Si in a constant area ratio of 0.2 on a reactivate atmosphere

of nitrogen and argon (purity of 99.9999%). The sputtering system was provided with flow meters to accurately control the argon and nitrogen flows into the deposition chamber. The growing coating time was of 2 h in all cases as well a dc power P of 200 W. Using mechanical and turbomolecular pumps, we obtained a maximum vacuum of 1×10^{-6} mbar while the AISI D2 tool steel and silicon substrate temperatures were controlled by thermopares at 400 °C. In order to obtain a good adherence between the coating and the substrate, a bombardment with positive ions (plasma) for 10 min. To obtain the Ti-Si-N-O coatings a metallic Ti-Si layer is deposited on the surface. Subsequently, the Ti-Si/substrate was hit at 400 °C (value at which the TiN oxides) and flows of N_2 were injected into the chamber in order to oxide the Ti-Si coating in order to form the Ti-Si-N-O quaternary system. The work pressure W_P was established at 8.9×10^{-3} mbar and the argon flow at F_{Ar} of 25 sccm. Table 1 summarizes the conditions during the Ti-Si-N-O on AISI D2 tool steel and silicon substrate growing process.

Structure and crystalline parameters of the Ti-Si-N-O coatings were obtained by XRD (model RIGAKU DMAX/1200), provided with a Cu $K\alpha_1$ radiation source (1.5406 Å) at an incidence angle of 5°. The chemical composition of the coatings was determined via EDS using an environmental SEM (PHILIPS XL30 ESEM). The indentation patterns produced during microhardness measurement and the thickness were observed by SEM. The microhardness of the coatings was measured by using a Vickers microhardness indenter (BRUEHLER Micromet 2100) under variable loads of 0.098, 0.245, 0.49, 0.98, 1.96, and 2.94 N. All the mechanical properties, including hardness, were carried out with a system Hysitron Ubi1 and they were performed in load control mode with a Berkovich tip and the values of hardness were corroborated by an indentation model proposed by Korsunsky (Ref 15). Surface morphology characterization was carried out using an AFM (Dimension 3100-Nanoscope IV of Digital Instruments).

3. The Indentation Model

In an experiment of indentation with a pyramidal sharp the highest applied load P, could be related to the maximum penetration depth δ by

$$P = \frac{H\delta^2}{k} \quad \text{(Eq 1)}$$

where k is a parameter describing the indenter geometry and H is the measured hardness. For Vickers indenter geometry, $\delta = d/7$, where d is the indent diagonal. If the depth δ is calculated in nanometers and the load P in Newton, then the hardness H is obtained in MPa (using the value $k = 0.3713$). The total energy W_{tot} required to produce an indentation of depth δ is then given by

$$W_{tot} = \int_0^{\delta} P\,dx = \frac{H\delta^3}{3k} \quad \text{(Eq 2)}$$

This is termed the "work of indentation" and experimentally can be used to define an effective value of H which usefully describes the resistance to deformation over the penetration δ. In terms of the work of indentation, the hardness is as follows:

$$H = \frac{3kW_{tot}}{\delta^3} \quad \text{(Eq 3)}$$

Also, the total energy could be composed of two parts: the plastic work of deformation in the substrate W_S, and the deformation and fracture energy in the coating W_C, given by

$$W_{tot} = W_S + W_C \quad \text{(Eq 4)}$$

It is convenient to define a dimensionless parameter β, given by the ratio between the indentation depth δ and the coating thickness t. It is sometimes called in the literature, the relative indentation depth (RID).

Considering the dependence of individual contributions on the relative indentation depth, coating and substrate properties, the following expression for H_{tot} (where H_{tot} is a function $H_{tot} = f(H_S, H_C, t, \beta, \text{etc.})$) can be derived:

$$H_{tot} = H_S + \frac{H_C - H_S}{1 + k\beta^2} \quad \text{(Eq 5)}$$

The total hardness (composite hardness) H_{tot} can be thought to depend only on the dimensionless parameters k and β, and the hardness difference between the coating and the substrate. Details of the model are presented in Ref 15.

Table 1 Growth parameters used to fabricate Ti-Si-N-O coating samples, where the work pressure, W_P, was 8.9×10^{-3} mbar for all samples

Sample	F_N, sccm	F_{Ar}, sccm	P, W	T, °C
F1TSN	3	25	200	400
F2TSN	5	25	200	400
F3TSN	7	25	200	400
F4TSN	9	25	200	400

4. Results and Discussion

Figure 1 shows the Ti-Si-N(O) coating metastable ternary phase diagram containing the chemical composition obtained via EDS. We found that the Ti-Si-N(O) coatings belong to the $TiSi_xN(O_y)$ and SiN_xO_y solid-solution region (Ref 11). The stoichiometry data reveal that the Ti-Si-N(O) fabricated coatings have a strong domain on titanium oxynitrure phase, which is related to the nitrogen flux used. The chemical composition for the F1TSN, F2TSN, F3TSN, and F4TSN samples are $Ti_{39.84}Si_{7.76}N_{27.56}0_{24.84}$, $Ti_{37.67}Si_{8.84}N_{29.04}0_{24.45}$, $Ti_{33.98}Si_{8.96}N_{38.9}0_{18.16}$, and $Ti_{30.35}Si_{9.45}N_{40.59}0_{19.61}$.

Figure 2 contains the diffraction patterns corresponding to the Ti-Si-N(O) coating samples fabricated under different flow rate conditions. We found that oxynitrure derivates into two different crystalline phases, fcc-TiN and fcc-$(TiO)_{3.38}$. We observed a phase transition from cubic titanium nitride to cubic titanium oxide as the nitrogen flow increases. In the case of F1TSN sample, we also found the presence of an AISI D2 tool steel substrate peak in $2\theta = 44.73°$. Both F1TSN and F2TSN coatings showed the fcc-TiN phase (JADE PDF-card # 38-1420) but preferential orientation in case of F1TSN was

(220) whereas sample F2TSN sample presented one at (200). In fact, the preferential orientation shown by F1TSN coating is ideal to use as a diffusion barrier when it is used in the fabrication of successful integrated circuits. It should be remarked that the crystalline preferential orientation of the columnar fcc-TiN structure is (111) or (200). Our study also shows that F3TSN and F4TSN samples present a preferential orientation at (220), where a phase transition from TiN to TiO is carried out. Actually, when temperature is applied to the substrate we observed the formation of fcc-TiO crystalline phase. Diffraction peaks identification demonstrates that it corresponds to cubic titanium oxide fcc-$(TiO)_{3.38}$ (JADE PDF-card # 75-0310). Also, Fig. 2 displays that an inverse relationship exists between peak intensity and nitrogen gas flow.

The Warren-Averbach method (Ref 16) was employed to analyze the diffraction peak line profile. Results are registered in Table 2. Again, we found an inverse relationship between the nitrogen flow and the fcc-TiN grain size until the crystalline phase fades. A similar behavior is observed in the case of fcc-$(TiO)_{3.38}$ phase. Similarly, the changes in width of the line at mid-height (FWMH) are related to the variation of the mean grain size as well as microdeformations.

We corroborated the results obtained by using XRD and EDS with the Raman scattering spectra studies for F1TSN, F2TSN, F3TSN, and F4TSN fabricated samples. Figure 3 shows the vibrational modes associated with Ti-N and Ti-O bonds (dot lines). Roughness mean square (RMS) of samples was obtained via AFM and they are presented together with the surface morphology in Fig. 4. RMS results oscillated from 9.83 to 21.77 nm. The high roughness is associated with the changes in titanium oxynitrure phase. We can observe that all samples present variable size cumulus that could change according to the crystalline phase present in them. Nevertheless, it is possible to appreciate at least two different types of color contrasts indicating the presence of two solid phases, one is crystalline and the other is amorphous.

It is necessary to take into account that neither XRD nor the Raman dispersion spectroscopy gives information with respect

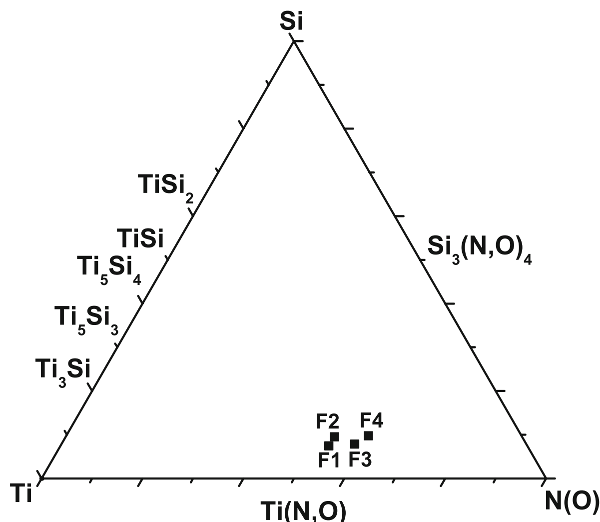

Fig. 1 The metastable ternary phase diagram of Ti-Si-N(O) coatings

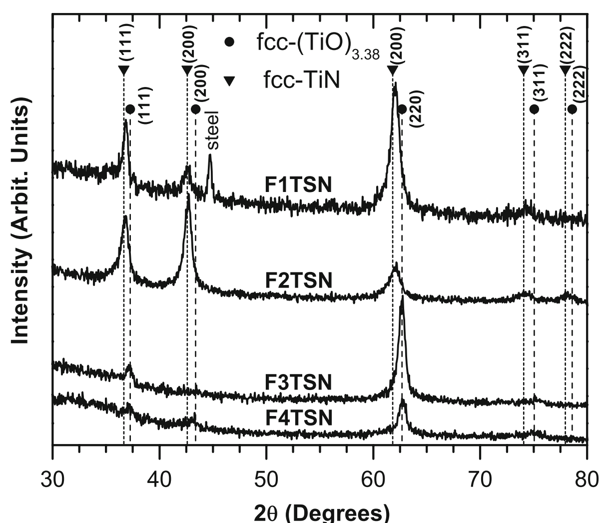

Fig. 2 X-ray diffraction pattern of all samples fabricated by reactive co-sputtering

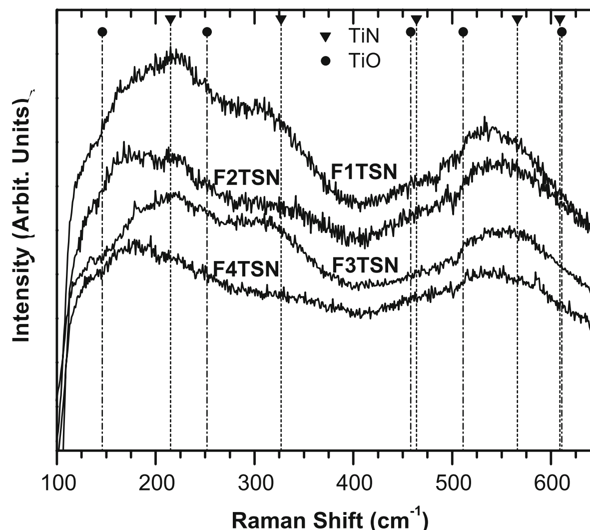

Fig. 3 Raman scattering spectra of the sample sets with substrate temperature of 400 °C

Table 2 Parameters obtained by Warren-Averbach method

Sample	Nitrogen flux, sccm	$2\theta_{(200)}$ TiN, °	FWHM TiN, °	Grain size, nm, TiN	$2\theta_{(200)}$ $(TiO)_{3.38}$, °	FWHM $(TiO)_{3.38}$, °	Grain size, nm, $(TiO)_{3.38}$
F1TSN	3	62.077	0.974	5.2	⋯	⋯	⋯
F2TSN	5	61.420	2.556	3	62.104	1.059	5.8
F3TSN	7	62.741	1.300	4.3	62.695	0.538	11.8
F4TSN	9	⋯	⋯	⋯	62.796	0.874	5.5

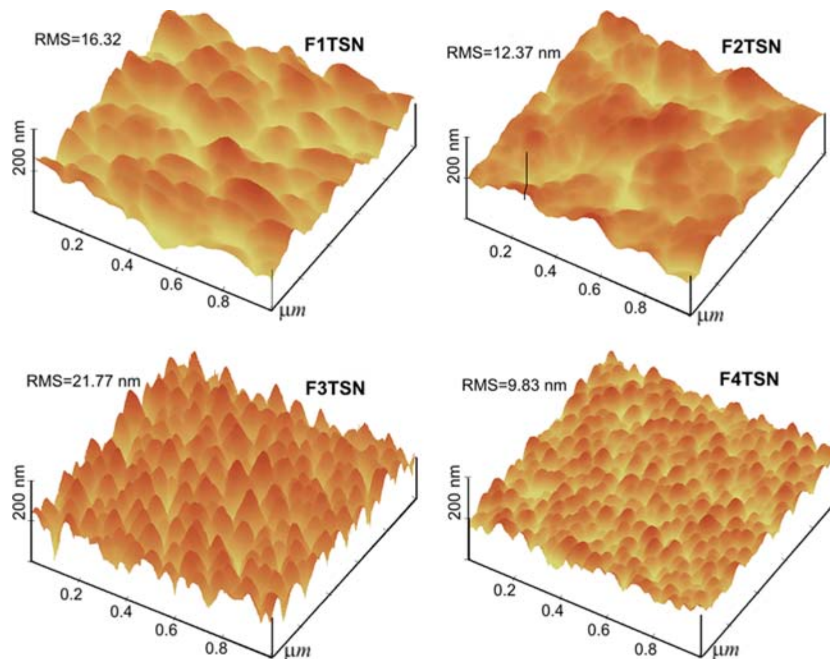

Fig. 4 AFM images of the surface of the samples in an area of 1.0 × 1.0 μm^2

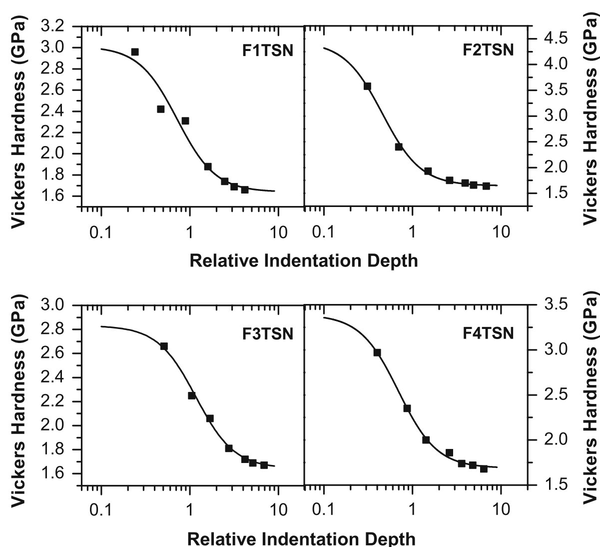

Fig. 5 Variation of hardness with applied load, measured in a substrate-coating composite, applying the work of indentation model

to silicon. According to investigations reported in literature (Ref 17, 18), if EDS detects silicon then it is present as part of the coatings in the $Si_3(N,O)_4$ amorphous phase (Ref 11). These results agree with the obtained stoichiometry of the coatings by EDS.

The indentation work model proposed by Korsunsky (Ref 19) was used to analyze the hardness variation within the full load range and indentation depths considered. The behavior obtained for each sample is shown in Fig. 5. Korsunsky's model describes the hardness variation in a coating/substrate system developed on a wide range of indentation loads and the relative indentation depths. The model does not assume either brittle or ductile coating responses, and can be applied with equal success to both types of coated systems. Korsunsky in this model shows that coating plasticity dominates the response at low loads, but if penetration increases then coating fracture occurs.

In the hardness analysis of Ti-Si-N-O coatings, the seven lower loads of Vickers indenter were performed and then the hardness was plotted against relative indentation depth, denoted by β. When a logarithmic scale is used for β, a characteristic knee shaped profile is observed, as shown in Fig. 5. Under the lowest loads, and in the absence of fracture under the indenter, the curve approaches the value of real coating hardness. This obtained behavior exceeds one-tenth the coating thickness, which means that the value of the obtained hardness is influenced by a great contribution of the substrate. The results obtained shows that the F2TSN sample presented the greatest hardness, behavior that agrees with the preferential crystalline orientation (200), typical columnar structure of the TiN, and with the highest relative texture coefficient for the peak (200). Also, the hardness is related with resistivity. In other words, the sample with highest hardness presented the lowest resistivity (F2TSN). Finally, although the F2TSN sample does not show the smallest grain size for the fcc-TiN phase, it is the only one that presents a pure fcc-TiN crystalline phase. Table 3 summarize the resistivity, thickness, hardness, Young's modulus, elastic recovery, and ratio *H*/*E* results for the several samples under study. The results show that the relationship between hardness and Young's modulus in Ti-Si-N-O coatings can be controlled by the choice of its chemical composition and deposition parameters. Hence, it is possible to tailor coatings with prescribed mechanical properties for a given application. In general, the Young's modulus increases when hardness increases. The same ratio *E*/*H* approximately correlates with the same elastic recovery. The most important finding that follows from the Ti-Si-N-O coatings is the fact that even with very different hardness it can exhibit the same

Table 3 **Resistivity, thickness, hardness, Young's modulus, elastic recovery, and ratio *H*/*E* by Ti-Si-N-O coatings**

Sample	Resistivity, μΩcm	Thickness, μm	Hardness, GPa	Young's modulus, GPa	Elastic recovery, %	Ratio *H*/*E*
F1TSN	1.02×10^8	2.28	3.0 ± 0.2	119.7 ± 1.5	31.6 ± 0.2	0.03
F2TSN	3.36×10^5	1.51	4.4 ± 0.5	138.1 ± 2.5	31.5 ± 0.3	0.03
F3TSN	2.27×10^6	1.48	2.8 ± 0.1	111.1 ± 0.5	31.1 ± 0.5	0.03
F4TSN	2.72×10^6	1.60	3.4 ± 0.1	113.9 ± 1.2	31.9 ± 0.3	0.03

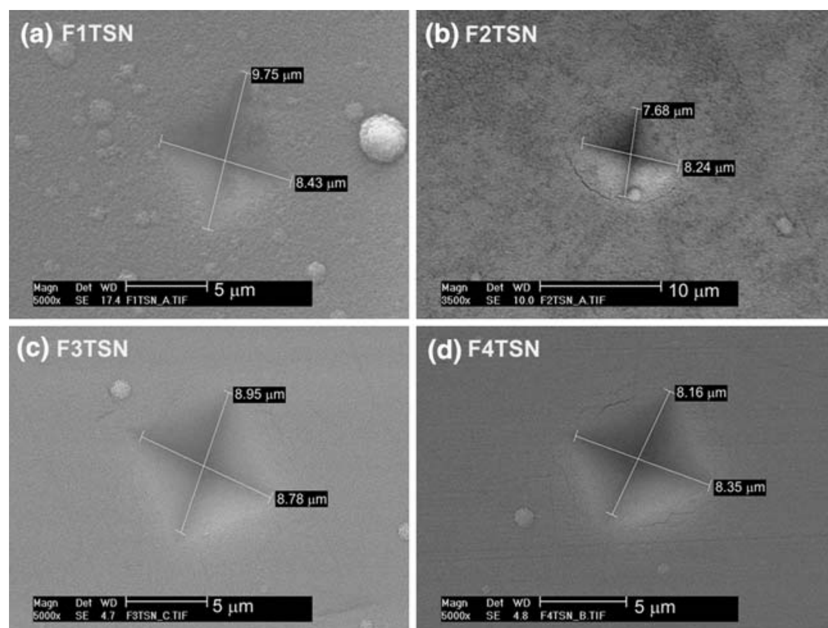

Fig. 6 Electron scanning microscopy images showing the indentation impressions produced with a load of 0.098 N in the samples: (a) F1TSN, (b) F2TSN, (c) F3TSN, and (d) F4TSN

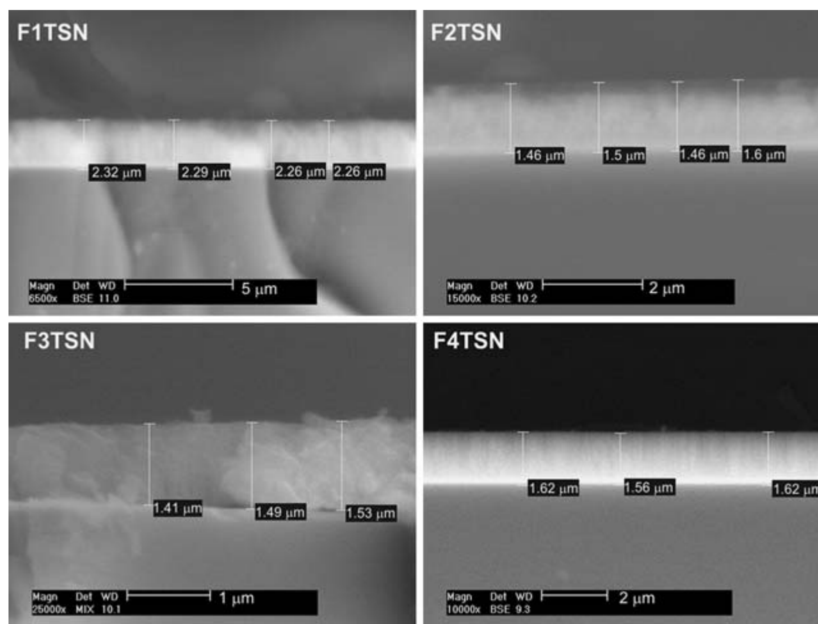

Fig. 7 SEM images of the cross section of the Ti-Si-N-O coating

elastic recovery, provided that the ratio *H*/*E* is approximately constant. Therefore, the properties of the Ti-Si-N-O coatings are closely connected to its structure, the which in turn, depends on the phase and chemical composition of the material, and this in turn is strongly dependent on the nitrogen content.

Electron scanning microscopy images of the indentation impressions produced by a load of 0.098 N are shown in Fig. 6 for (a) F1TSN, (b) F2TSN, (c) F3TSN, and (d) F4TSN. The behavior shown in these images indicates that in the two harder samples, F2TSN and F4TSN, the indentation cracks appear only at the contact site and there are visible cracks around the indenter impression. These successive lateral cracks on each side of the Vickers indenter impression remain roughly parallel to the contact edge between indenter and sample surface. A few nested cracks and sinking-in effect visible in this images around the contact edge are due to local delamination between coatings and substrate. Finally, in Fig. 7 thickness values can be deduced from the SEM micrographs and the cross section of the Ti-Si-N-O coatings is observed. The thickness is obtained via the measurement of contrast phase by SEM-EDS. The difference of phase contrasts allows to differentiate the interface between the coatings and the substrates. The cross section corroborates the high homogeneity of the coatings surface after the deposition process.

So, it should be noted that the grain size is not the only parameter necessary to explain the variations of the coating hardness in the quaternary systems. The structural changes related to chemical composition and hardness of each coating are very important factors that directly influence bond energy, which is manifested to resist the deformation under an applied load.

5. Conclusions

The structure, chemical composition, and hardness of Ti-Si-N-O coatings prepared by dc reactive magnetron sputtering are strongly influenced by the nitrogen flow. The crystalline part of this quaternary system was dominated by the titanium oxynitride. By using a nitrogen flow rate of 5 sccm, F2TSN sample, was able to obtain the columnar structure of fcc-TiN with a preferential orientation of (200). In fact, (200) is a typical orientation where fcc-TiN presents the highest hardness value, which is in agreement with our results. Also, F2TSN sample presented the smallest value for resistivity. The remaining samples presented a (220) preferential crystalline orientation, a favorable orientation to have a greater resistivity value. The Ti-Si-N-O coating presented different hardness but exhibited the same elastic recovery and the same value of the ratio H/E. In fact, our samples have shown a quasi-linear correlation between the ratio H/E and the elastic recovery.

Acknowledgments

This work was supported by CONACYT by means of the project 58653. Authors gratefully acknowledge Pedro García Jiménez and José Eleazar Urbina Álvarez at CINVESTAV Unidad Querétaro, as well as, Marcela Guerrero and Ana B. Soto at Departamento de Física - CINVESTAV, for their technical assistance.

References

1. S.H. Kim, J.W. Jang, S.S. Kang, and K.H. Kim, Synthesis and Mechanical Evaluation of Nanocomposite Coating Layer of nc-TiN/a-Si_3N_4 on SKD 11 Steel by Sputtering, *J. Mater. Process. Technol.*, 2002, **130–131**, p 283–288 in English
2. H. Watanabe, Y. Sato, Ch. Nie, A. Ando, S. Ohtani, and N. Iwamoto, The Mechanical Properties and Microstructure of Ti-Si-N Nanocomposite Coatings by Ion Plating, *Surf. Coat. Technol.*, 2003, **169–170**, p 452–455 in English
3. J.S. Reid, E. Kolawa, C.M. Garland, M.-A. Nicolet, F. Cardone, D. Gupta, and R.P. Ruiz, Amorphous (Mo, Ta, or W)-Si-N Diffusion Barriers for Al Metallizations, *J. Appl. Phys.*, 1996, **79**(2), p 1109–1115 in English
4. K. Nakajima, Y. Akasaka, K. Miyano, M. Takahashi, S. Suehiro, and K. Suguro, Formation Mechanism of Ultrathin WSiN Barrier Layer in a W/WN_x/Si System, *Appl. Surf. Sci.*, 1997, **117–118**, p 312–316 in English
5. F. Letendu, M.C. Hugon, B. Agius, I. Vickridge, C. Berthier, and J.M. Lameille, TaSiN Diffusion Barriers Deposited by Reactive Magnetron Sputtering, *Thin Solid Films*, 2006, **513**(1–2), p 118–124 in English
6. Y.-J. Lee, B.-S. Suh, M.-S. Kwon, and C.-O. Park, Barrier Properties and Failure Mechanism of Ta-Si-N Thin films for Cu Interconnection, *J. Appl. Phys.*, 1999, **85**(3), p 1927–1934 in English
7. J. Bonitz, R. Ecke, S.E. Schulz, and T. Gessner, Different SiH_4 Treatments of CVD TiN Barrier Layers, *Microelectron. Eng.*, 2005, **82**(3–4), p 618–622 in English
8. H.-E. Cheng, W.-J. Lee, and C.-M. Hsu, The Effect of Deposition Temperature on the Properties of TiN Diffusion Barriers Prepared by Atomic Layer Chemical Vapor Deposition, *Thin Solid Films*, 2005, **485**(1–2), p 59–65 in English
9. L. Gao, J. Li, T. Kusunose, and K. Niihara, Preparation and Properties of TiN-Si_3N_4 Composites, *J. Eur. Ceram. Soc.*, 2004, **24**(2), p 381–386 in English
10. J. Procházka, P. Karvánková, M.G.J. Vepřek-Heijman, and S. Vepřek, Conditions Required for Achieving Superhardness of ≥45 GPa in nc-TiN/a-Si_3N_4 Nanocomposites, *Mater. Sci. Eng. A*, 2004, **384**(1–2), p 102–116, in English
11. E.V. Shalaeva, S.V. Borisov, O.F. Denisov, and M.V. Kuznetsov, Metastable Phase Diagram of Ti-Si-N(O) Films ($C_{Si} < 30$ at.%), *Thin Solid Films*, 1999, **339**(1–2), p 129–136 in English
12. Y.C. Ee, Z. Chen, T.M. Lu, Z.L. Dong, and S.B. Law, Low Temperature Physical-Chemical Vapor Deposition of Ti-Si-N-O Barrier Films, *Electrochem. Solid-State Lett.*, 2006, **9**(3), p G100–G103 in English
13. P.M. Smith and J.S. Custer, Chemical Vapor Deposition of Titanium-Silicon-Nitride Films, *Appl. Phys. Lett.*, 1997, **70**(23), p 3116–3118 in English
14. Y.C. Ee, Z. Chen, S.B. Law, and S. Xu, Formation and Characterization of Ti-Si-N-O Barrier Films, *Thin Solid Films*, 2006, **504**(1–2), p 218–222 in English
15. A.M. Korsunsky, M.R. McGurk, S.J. Bull, and T.F. Page, On the Hardness of Coated System, *Surf. Coat. Technol.*, 1998, **99**(1–2), p 171–183 in English
16. M. McKeehan and B.E. Warren, X-Ray Study of Cold Work in Thoriated Tungsten, *J. Appl. Phys.*, 1953, **24**(1), p 52–56 in English
17. C. Louro and A. Cavaleiro, Mechanical Behaviour of Amorphous W-Si-N Sputtered Films After Thermal Annealing at Increasing Temperatures, *Surf. Coat. Technol.*, 2000, **123**(2–3), p 192–198 in English
18. S. Vepřek and S. Reiprich, A Concept for the Design of Novel Superhard Coatings, *Thin Solid Films*, 1995, **268**(1–2), p 64–71 in English
19. J.R. Tuck, A.M. Korsunsky, R.I. Davidson, S.J. Bull, and D.M. Elliott, Modelling of the Hardness of Electroplated Nickel Coatings on Copper Substrates, *Surf. Coat. Technol.*, 2000, **127**, p 1–8 in English